SUPPLEMENT MATERIAL for: Dynamic Group-Aware Bayesian Shrinkage and Redundancy-Aware Screening in Spatial Panel Models

1 Spatial Units and Candidate Variables

Table 1 reports the spatial units included in the empirical panel, while Table 2 reports the candidate covariates used after alignment with the empirical specification and their group assignments. These groups define the hierarchical shrinkage structure used in the Bayesian model; posterior relevance and redundancy-aware pruning are then determined from the estimated model.

Table 1: Spatial units included in the empirical panel.

Austria	Belgium	Lithuania	Luxembourg
Bulgaria	Croatia	Malta	Netherlands
Cyprus	Czechia	Norway	Poland
Denmark	Estonia	Portugal	Romania
Finland	France	Slovakia	Slovenia
Germany	Greece	Spain	Sweden
Hungary	Ireland	Italy	Latvia

Table 2: Candidate variables and group assignments used in the empirical analysis.

Variable	Description	Group
ren_ene_sh	Renewable energy share	renewable energy
ren_el_sh	Renewable energy share in electricity	renewable energy
ren_trans_sh	Renewable energy share in transport	renewable energy
renen_el_sh	Renewables share in electricity production	renewable energy
elprice_h	Household electricity price	energy prices
elprice_nnh	Non-household electricity price	energy prices
gas_price_notax	Gas price excluding taxes	energy prices
gas_price_tax	Gas price including taxes	energy prices
pop	Population	macro-structural conditions
gfcf_pc	Gross fixed capital formation per capita	macro-structural conditions
gdp_pc_gr	GDP per capita growth	macro-structural conditions
el_imp	Electricity imports	energy trade and dependence
ene_imp	Energy import dependence	energy trade and dependence
imp_oil	Oil and petroleum imports	energy trade and dependence
el_exp	Electricity exports	energy trade and dependence
prod_el_renfuel	Electricity production from renewables and biofuels	electricity production structure
prod_el_solid	Electricity production from solid fossil fuels	electricity production structure
prod_el_fossilheat	Electricity production from fossil heat sources	electricity production structure
prod_el_fossilheat_pc	Electricity production from fossil heat sources per capita	electricity production structure
ene_intgdp_vol	Energy intensity of GDP	system efficiency and competitiveness
prod	Productivity indicator	system efficiency and competitiveness
comp_country	Cross-border electricity-market competitiveness indicator	system efficiency and competitiveness
int_country	Cross-border electricity-market integration indicator	system efficiency and competitiveness
tot_env_taxes	Total environmental taxes	environmental and fiscal pressure
ghg_tot_pc	Total greenhouse-gas emissions per capita	environmental and fiscal pressure
ghg_ene_pc	Energy-related greenhouse-gas emissions per capita	environmental and fiscal pressure
ar_uti_bills	Arrears on utility bills	social and housing vulnerability
cost_disphouseinc_sh	Housing costs in disposable household income	social and housing vulnerability
house_deprate_city	Housing deprivation rate in cities	social and housing vulnerability
house_deprate_rural	Housing deprivation rate in rural areas	social and housing vulnerability
risk_poverty	Risk of poverty	social and housing vulnerability

Notes: The empirical variables are obtained from the *Eurostat* database. Group labels refer to the domains used in the group-aware shrinkage component.

2 Additional Computational Diagnostics and Screening Evidence

2.1 MCMC Diagnostics

Table 3 reports chain-level posterior summaries and acceptance rates for the full-sample estimation (Gelman et al. 1995; Plummer et al. 2006; Brooks et al. 2011). The four chains display closely aligned posterior moments for the main quantities reported in the table. The posterior mean of ρ_t is concentrated around 0.216 across chains, while the posterior mean of σ_t^2 ranges only from 0.668 to 0.672. The global shrinkage scale τ^2 also remains small and stable across chains. Acceptance rates are similar across chains, with average Metropolis-Hastings acceptance close to 0.594 for the log-variance block and 0.552 for the spatial autoregressive block. These summaries indicate that the posterior output is not driven by chain-specific behaviour or seed choice.

Figure 1 compares posterior credible intervals and bootstrap-based intervals for the dynamic spatial dependence parameter ρ_t. The two interval constructions support the same temporal pattern, with stronger spatial dependence in the earlier part of the sample, lower values in the middle years, and a partial increase towards the end. Bootstrap intervals are wider in some periods, but they do not change the interpretation of the estimated spatial-dependence path.

Table 3: Chain-level MCMC summary statistics and acceptance rates for the full-sample estimation.

Chain	Seed	Elapsed sec.	$\bar{\rho}$	sd(ρ)	$\bar{\sigma}^2$	sd(σ^2)	$\bar{\tau}^2$	Acc. SV	Acc. ρ
chain_1	2025	30839.66	0.217	0.129	0.668	1.333	0.001	0.594	0.552
chain_2	2026	30448.86	0.216	0.130	0.671	1.348	0.002	0.594	0.551
chain_3	2027	28502.90	0.217	0.130	0.672	1.352	0.002	0.594	0.552
chain_4	2028	28901.19	0.217	0.130	0.672	1.344	0.002	0.594	0.552

Notes: The table reports chain-specific posterior means, posterior standard deviations, elapsed computing time, and average Metropolis-Hastings acceptance rates for the stochastic-variance and spatial-autoregressive updates.

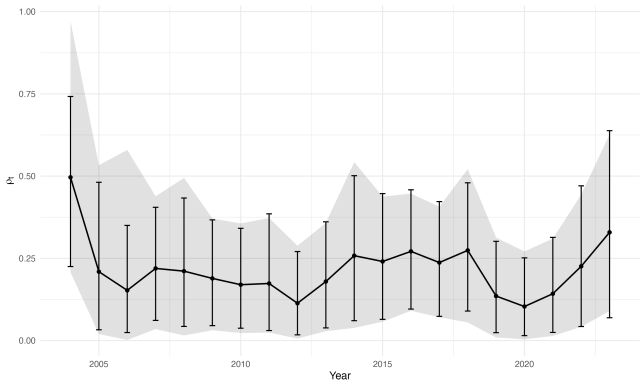

Fig. 1: Uncertainty diagnostics for the time-varying spatial dependence parameter ρ_t. The solid line denotes the posterior mean, the shaded region denotes posterior credible intervals, and the vertical bars denote bootstrap-based intervals.

Figure 2 reports posterior densities for average spatial dependence, average observational variance, the global shrinkage scale, and the group-specific shrinkage scales. The marginal posterior distributions are unimodal and show no irregular shapes. Average spatial dependence is concentrated on positive values, while the variance and shrinkage-scale distributions show the expected right-tail behaviour of positive parameters.

Figure 3 provides diagnostics for the group-specific shrinkage scales ϕ_g^2. Posterior locations differ across groups, with larger values for system efficiency and competitiveness, energy trade and dependence, and electricity production structure. The trace plots show some local variability, but no persistent separation across chains or systematic drift, supporting the stability of the group-aware shrinkage component.

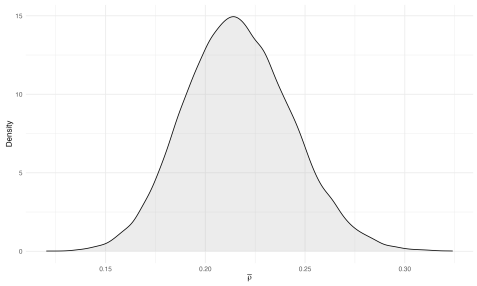

(a) Average spatial dependence.

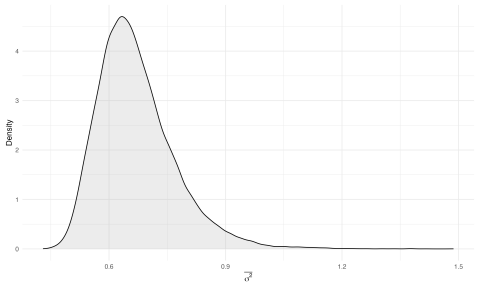

(b) Average observational variance.

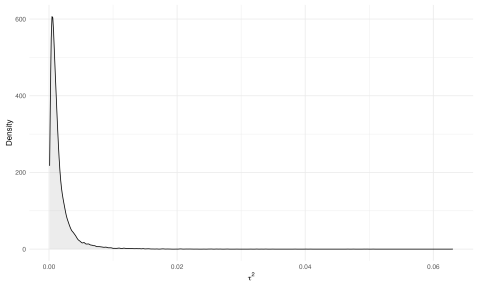

(c) Global shrinkage scale τ^2.

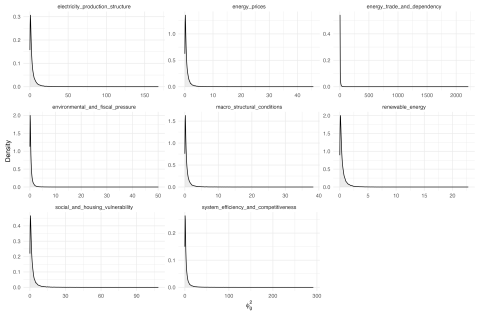

(d) Group-specific shrinkage scales ϕ_g^2.

Fig. 2: Posterior densities of the main shrinkage and dependence components.

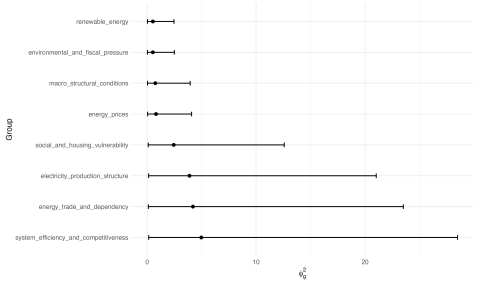

(a) Posterior summaries for ϕ_g^2.

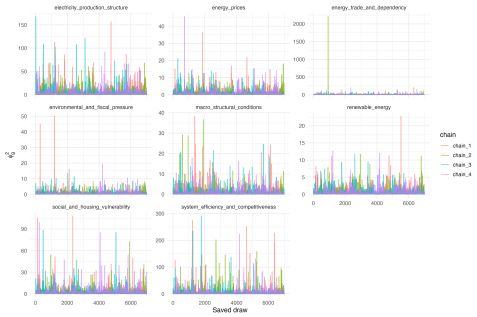

(b) Trace plots for ϕ_g^2.

Fig. 3: Diagnostics for the group-specific shrinkage scales ϕ_g^2. Panel (a) reports posterior means and 95% credible intervals. Panel (b) reports the corresponding trace plots.

2.2 Group-Level Screening Summaries

Table 4 reports additional group-level summaries of posterior relevance, signal intensity, and group-specific shrinkage. The table links the relevance structure from DPRP-based screening to the hierarchical shrinkage layer estimated in the Bayesian model.

The strongest average posterior relevance is found for social and housing vulnerability, followed by energy prices. By contrast, energy trade and dependence, electricity production structure, and system efficiency and competitiveness display larger posterior values of ϕ_g^2, indicating greater dynamic flexibility for these groups. Posterior relevance and group-level shrinkage intensity therefore capture related but distinct features of the fitted model.

Table 4: Group-level summary of dynamic posterior relevance and group-specific shrinkage.

Group	No. vars.	DPRP mean	DPRP median	Signal mean	ϕ_g^2 mean	ϕ_g^2 median
Social and housing vulnerability	5	0.960	0.998	6.950	2.441	1.204
Energy prices	4	0.908	0.893	2.957	0.816	0.412
Energy trade and dependence	4	0.788	0.827	4.586	4.201	1.530
Electricity production structure	4	0.783	0.814	3.002	3.887	1.793
Environmental and fiscal pressure	3	0.757	0.793	1.963	0.524	0.269
Renewable energy	4	0.683	0.630	1.600	0.524	0.283
System efficiency and competitiveness	4	0.652	0.554	1.702	4.968	1.915
Macro-structural conditions	3	0.597	0.549	0.996	0.750	0.347

Notes: Group-level DPRP statistics are obtained by aggregating variable-level posterior relevance measures within each group. Signal mean denotes the average signal-to-threshold ratio. The last two columns report posterior summaries of the group-specific shrinkage scale ϕ_g^2.

2.3 Sign and Selection Stability under Top-1 and Top-2 Refits

Table 5 reports sign and selection stability under the *top-1* and *top-2* refits. In the *top-1* refit, `risk_poverty`, `el_imp`, `imp_oil`, and `house_deprate_rural` remain sign-stable, while `ren_ene_sh` is less stable under the more compact reduction. In the *top-2* refit, the most stable variables are `risk_poverty`, `prod`, `el_imp`, `house_deprate_rural`, and `house_deprate_city`. Other retained predictors remain relevant but are more sensitive to the reduced specification considered.

Overall, the evidence identifies a stable core of vulnerability, electricity-import, and productivity-related predictors, while the remaining *top-2* variables are more sensitive to the refitted specification.

Table 5: Sign and selection stability under the *top-1* and *top-2* refits.

Spec.	Variable	Sign share	Full DPRP	Reduced DPRP	DPRP diff.	Reduced $\lvert\beta\rvert$
top-1	risk_poverty	1.000	1.000	1.000	0.000	0.676
top-1	el_imp	1.000	0.998	1.000	0.001	0.235
top-1	imp_oil	1.000	0.999	0.990	-0.009	0.109
top-1	house_deprate_rural	1.000	0.999	0.958	-0.041	0.097
top-1	ren_ene_sh	0.000	0.967	0.570	-0.397	0.014
top-2	risk_poverty	1.000	1.000	1.000	0.000	0.601
top-2	prod	1.000	0.999	1.000	0.001	0.217
top-2	el_imp	1.000	0.998	1.000	0.001	0.269
top-2	house_deprate_rural	1.000	0.999	1.000	0.001	0.289
top-2	house_deprate_city	1.000	0.998	1.000	0.001	0.232
top-2	prod_el_solid	0.000	1.000	0.877	-0.122	0.066
top-2	ren_ene_sh	0.000	0.967	0.864	-0.102	0.046
top-2	imp_oil	1.000	0.999	0.754	-0.245	0.049
top-2	gas_price_notax	0.000	0.957	0.588	-0.369	0.014

Notes: Sign share denotes the share of time periods in which the coefficient sign agrees between the full and reduced refits. Reduced DPRP is the mean DPRP under the refitted reduced specification. DPRP diff. is the difference between reduced-model and full-model DPRP means.

2.4 Threshold-Robust Group-Level Screening Patterns

Table 6 summarises how the group structure represented in the baseline *top-2* specification changes when the practical-significance threshold is varied. The table is restricted to groups represented in the preferred *top-2* model.

The social and housing vulnerability group remains the most robust block across threshold values. It contributes three selected variables under $c = 0.5$ and $c = 1.0$, and two variables under the stricter threshold $c = 1.5$. Energy trade and dependence also remains represented under the stricter threshold, although with fewer selected variables. By contrast, renewable energy, energy prices, and electricity production lose their selected representatives when c is raised to 1.5. The contraction under the stricter rule is therefore structured, preserving the most persistent social-vulnerability and external-exposure components.

Table 6: Group-level robustness of the *top-2* specification under alternative practical-significance thresholds.

c	Group	Top-2 selected	Avg. DPRP	Avg. signal	Avg. abs. β
0.5	Electricity production structure	1	0.891	6.003	0.301
0.5	Energy prices	1	0.960	5.913	0.115
0.5	Energy trade and dependence	2	0.891	9.172	0.265
0.5	Renewable energy	1	0.837	3.201	0.085
0.5	Social and housing vulnerability	3	0.982	13.901	0.291
0.5	System efficiency and competitiveness	1	0.819	3.404	0.156
1.0	Electricity production structure	1	0.783	3.002	0.301
1.0	Energy prices	1	0.908	2.957	0.115
1.0	Energy trade and dependence	2	0.788	4.586	0.265
1.0	Renewable energy	1	0.683	1.600	0.085
1.0	Social and housing vulnerability	3	0.960	6.950	0.291
1.0	System efficiency and competitiveness	1	0.652	1.702	0.156
1.5	Electricity production structure	0	0.677	2.001	0.301
1.5	Energy prices	0	0.834	1.971	0.115
1.5	Energy trade and dependence	1	0.701	3.057	0.265
1.5	Renewable energy	0	0.545	1.067	0.085
1.5	Social and housing vulnerability	2	0.931	4.634	0.291
1.5	System efficiency and competitiveness	1	0.516	1.135	0.156

Notes: Top-2 selected denotes the number of retained variables from each group. DPRP, signal, and absolute coefficient magnitude are averaged within group.

2.5 Fuzzy-Partition Robustness Diagnostics

Figure 4 reports the full membership matrix for the selected fuzzy partition, showing both dominant and partial memberships across profiles. The block structure indicates that most units have a prevailing profile, while some countries retain secondary memberships in other clusters. The partition therefore shows a clear structure without reducing all units to fully crisp assignments.

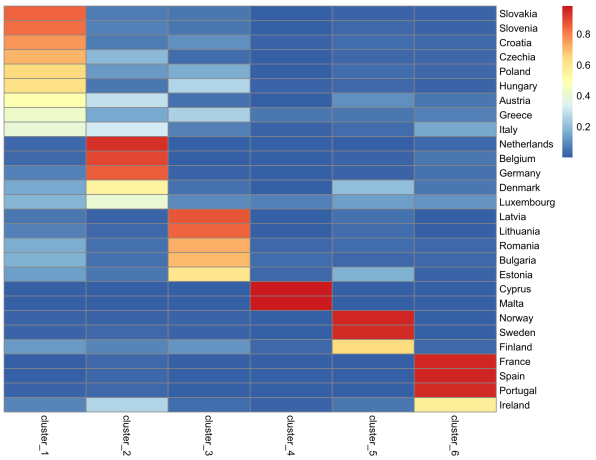

Fig. 4: Membership matrix under the selected spatially weighted dynamic fuzzy partition.

Table 7 and Figure 5 report cluster-overlap diagnostics between the baseline fuzzy partition and the alternative specifications. Under uniform weights, the large baseline clusters are reproduced without changes. Under the $k = 5$ restriction, the main clusters are still identifiable, although some of them are combined. Baseline cluster 2 shows the lowest overlap, indicating greater sensitivity to the smaller number of clusters.

Table 7: Overlap between large baseline clusters and best-matching clusters under admissible alternatives.

Comparison	Baseline cl.	Size	Overlap	Precision	Jaccard
Baseline vs best $k = 5$	1	9	7	0.778	0.700
Baseline vs best $k = 5$	2	5	3	0.600	0.333
Baseline vs best $k = 5$	3	5	3	0.600	0.600
Baseline vs best $k = 5$	6	4	4	1.000	0.571
Baseline vs best uniform	1	9	9	1.000	1.000
Baseline vs best uniform	2	5	5	1.000	1.000
Baseline vs best uniform	3	5	5	1.000	1.000
Baseline vs best uniform	6	4	4	1.000	1.000

Notes: Only baseline clusters with at least four units are reported. Overlap denotes the number of common units between each baseline cluster and its best-matching alternative cluster. Precision is the share of the baseline cluster recovered in the matched cluster. Jaccard overlap is computed on the union of the two sets.

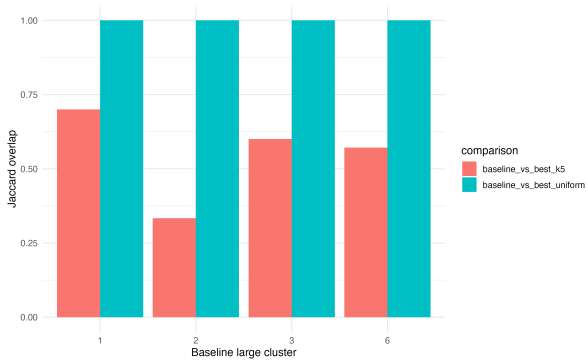

Fig. 5: Jaccard overlap between large baseline clusters and their best-matching counterparts under admissible alternatives.

The baseline partition also includes a two-unit cluster containing Cyprus and Malta. Table 8 reports that the two countries remain grouped together under both alternative specifications, with mean maximum membership equal to 0.975 in the baseline solution. This suggests a well-defined small profile rather than a residual or unstable grouping.

Table 8: Robustness of the baseline micro-cluster.

Cluster	Units	Mean max. memb.	Best $k = 5$	Best uniform
4	Cyprus, Malta	0.975	Preserved	Preserved

Notes: Preservation indicates whether the same two units remain grouped together under the corresponding alternative specification.

3 Additional Predictive Validation Evidence

3.1 Calibration and Temporal Error Profiles

Figure 6 reports two diagnostics for the four validation models. Panel (a) compares observed and predicted values over the full validation sample. The unrestricted full model and the posterior-screened *top-2* model both reproduce the main signal in the data, while the fuzzy-interaction specification shows the closest alignment with the 45-degree line. The additive fuzzy specification does not show a visible calibration gain relative to the *top-2* benchmark. Panel (b) reports annual RMSE profiles. The fuzzy-interaction model performs particularly well over the central part of the validation period, where its RMSE is lower than that of the competing specifications for several consecutive years. Its advantage weakens in the final part of the sample, where the *top-2* benchmark becomes more competitive. This indicates that the predictive contribution of latent heterogeneous responses is relevant but time-varying.

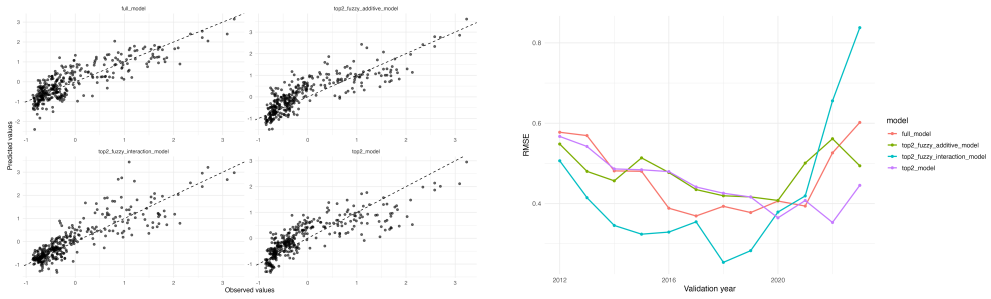

(a) Observed versus predicted values. **(b)** Year-specific RMSE profiles.

Fig. 6: Predictive calibration and annual RMSE profiles for the four validation models.

3.2 Sensitivity to Individual Validation Years

Figure 7 reports a leave-one-year-out diagnostic. Each validation year is omitted in turn, and the percentage improvement of the fuzzy-interaction specification is recomputed relative to the full and *top-2* benchmarks.

The MAE gains remain positive regardless of which single year is removed, indicating that the improvement in typical prediction error is not driven by one validation year. RMSE gains are more sensitive to the later years of the sample. The gain relative

to the full model remains positive throughout, whereas the gain relative to the *top-2* benchmark increases when some final validation years are omitted. The pattern indicates that the fuzzy-interaction specification improves prediction over most validation years, although the gains are smaller near the end of the sample.

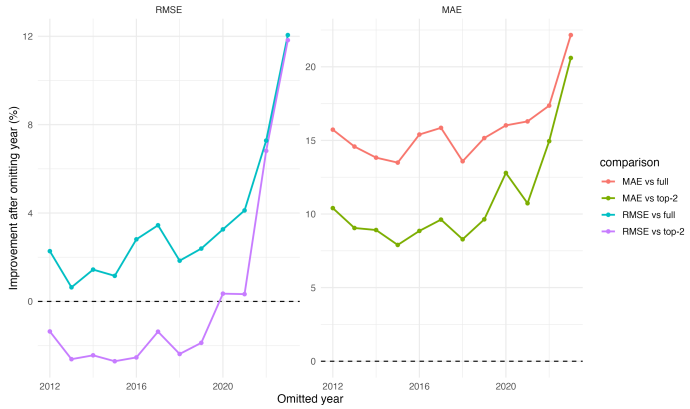

Fig. 7: Leave-one-year-out sensitivity analysis for the fuzzy-interaction specification.

References

Brooks, S., Gelman, A., Jones, G., Meng, X.-L. (eds.): Handbook of Markov Chain Monte Carlo. CRC press, Boca Raton (2011)

Gelman, A., Carlin, J.B., Stern, H.S., Rubin, D.B.: Bayesian Data Analysis, 1st edn. Chapman and Hall/CRC, Boca Raton (1995). https://doi.org/10.1201/9780429258411

Plummer, M., Best, N., Cowles, K., Vines, K.: Coda: Convergence diagnosis and output analysis for mcmc. R News **6**(1), 7–11 (2006)